Title

Observation of the topological surface state in the nonsymmorphic topological insulator KHgSb

Journal

Physical Review B, 96(16)

ISSN

2469-9950

Authors

Liang, AJ

Jiang, J

Wang, MX

et al.

Publication Date

2017-10-01

DOI

10.1103/physrevb.96.165143

Peer reviewed

Observation of the Topological Surface State in the Nonsymmorphic Topological Insulator KHgSb

A. J. Liang[1†], J. Jiang[1,2,3†], M. X. Wang[1], Y. Sun[4], N. Kumar[4], C. Shekhar[4], C. Chen[5], H. Peng[5], C. W. Wang[6], H. F. Yang[1,6], S. T. Cui[1], G. H. Hong[1], Y.-Y. Xia[1,4], S.-K. Mo[2], Q. Gao[7], X. J. Zhou[7,8], L. X. Yang[9], C. Felser[4], B. H. Yan[10], Z. K. Liu[1*] and Y. L. Chen[1,5,9,11*]

[1]*School of Physical Science and Technology, ShanghaiTech University, Shanghai, P. R. China*

[2]*Advanced Light Source, Lawrence Berkeley National Laboratory, Berkeley, CA 94720, USA*

[3]*Pohang Accelerator Laboratory, POSTECH, Pohang 790-784, Korea*

[4]*Max Planck Institute for Chemical Physics of Solids, D-01187 Dresden, Germany*

[5]*Department of Physics, University of Oxford, Oxford, OX1 3PU, UK*

[6]*State Key Laboratory of Functional Materials for Informatics, SIMIT, Chinese Academy of Sciences, Shanghai 200050, P. R. China*

[7]*Beijing National Laboratory for Condensed Matter Physics, Institute of Physics, Chinese Academy of Sciences, Beijing 100190, P. R. China*

[8]*Collaborative Innovation Center of Quantum Matter, Beijing, P. R. China*

[9]*State Key Laboratory of Low Dimensional Quantum Physics, Department of Physics and Collaborative Innovation Center of Quantum Matter, Tsinghua University, Beijing 100084, P. R. China*

[10]*Department of Condensed Matter Physics, Weizmann Institute of Science, Rehovot 7610001, Israel*

[11]*Hefei Science Center, CAS and SCGY, University of Science and Technology of China, Hefei, P. R. China*

†These authors contributed equally to this work.

**Corresponding authors: liuzhk@shanghaitech.edu.cn, yulin.chen@physics.ox.ac.uk*

Topological insulators represent unusual topological quantum states, typically with gapped bulk band structure but gapless surface Dirac fermions protected by the time-reversal symmetry. Recently, a new kind of topological insulators result from the nonsymmorphic crystalline symmetry was proposed in the KHgX (X=As, Sb, Bi) compounds. Unlike regular topological crystalline insulators, the (nonsymmorphic) glide reflection symmetry in KHgX guarantees the appearance of an exotic surface fermion with hourglass shape dispersion (where two pairs of branches switched their partners) residing on its (010) side surface, contrasting to the usual 2D Dirac fermion form. Here, by using high resolution angle-resolved photoemission spectroscopy (ARPES), we systematically investigated the electronic structures of KHgSb on both (001) and (010) surfaces and reveal the unique quasi-one-dimensional like in gap surface states on the (010) surface with delicate dispersion consistent with the "hourglass Fermion" recently proposed. Our experiment confirms KHgSb as a nonsymmorphic topological crystalline insulator with hourglass fermions, which serves as an important step to the discovery of novel topological quantum materials and exotic fermions protected by the nonsymmorphic crystalline symmetry.

The investigation on novel topological quantum states, including topological insulators[1-8], topological crystalline insulators[9-14] and topological semimetals[15-32], has become one of the most intensively studied topics in condensed matter physics. These topological quantum states not only possess novel fermions (such as 2D and 3D Dirac fermions[1-23], Weyl Fermions[24-32] and Majorana Fermions[33-34]) which can host many fascinating physical phenomena (such as the QSH effect[4-5], QAH effect[35-36], and XMR[37-41]). Remarkably, as these novel fermions and phenomena are protected by symmetries (e.g. time-reversal symmetry and space-group symmetries), they are robust against perturbations.

Recently, the nonsymmorphic-symmetry-protected topological quantum states, including topological insulators and semimetals were under intensive research[42-52]. Among them, KHgX (X=As, Sb, Bi) compounds were proposed as the first family of nonsymmorphic topological insulator[49-51]. According to the *ab-initio* calculations[49], KHgX are insulating in the bulk but possess robust gapless surface states (see Fig. 1a), forming the unique "hourglass Fermions" on the (010) surface. The surface fermion contains four branches (quadruplets) dispersions and unbreakable zigzag chain-like patterns [49] (Fig. 1b). These surface states can also be understood as two copies of surface states of weak topological insulators[53]. The nonsymmorphic glide mirror protects these two copies from annihilating with each other inside the mirror plane. In order to visualize the intriguing hourglass fermion surface states and confirm the nonsymmorphic topological insulator nature of KHgX, ARPES is the natural experimental tool.

In this work, we report comprehensive ARPES study on the electronic structures of KHgSb on both (001) and (010) surfaces. From the (001) surface, we observed insulating bulk states over the whole Brillouin zone with an indirect band gap of ~200 meV without signature of the in-gap surface states. Remarkably, on the (010) surface, we observed clear in-gap quasi-one-dimensional surface states with dispersions consistent with the hourglass configuration, as proposed in the recent theoretical work[49]. The broad agreement between the experimental results and the *ab initio* calculations confirms KHgSb as a nonsymmorphic topological crystalline insulator, which serves as an important step to the discovery of novel topological quantum materials and exotic fermions protected by the nonsymmorphic crystalline symmetry.

Basic information of KHgSb

High quality KHgSb crystals was synthesized by the flux method (see Appendix for details). The crystal structure of KHgSb is shown in Fig. 1c with space group $P6_3/mmc$ and the lattice constants $a=b=4.78$ Å, $c=10.225$ Å. The in-plane Hg and Sb atoms show strong bonding,

forming in-plane honeycomb lattices. The off-plane K atoms sit above the center of each honeycomb, sandwiched loosely by the two adjacent layers and serve as their inversion center. The natural cleavage surface is along the (001) and (010) surface (parallel to the diagonal of the in-plane honeycomb and preserves the glide reflection). The bulk Brillouin zone (BZ) and the surface BZs of both (001) and (010) surfaces are shown in Fig. 1d. Fig. 1e, f illustrate the broad Fermi surface mapping across multiple BZs on the (001) and (010) surfaces, respectively, confirming the cleavage surfaces with correct lattice parameters (the momentum direction of k_x is defined along $\tilde{\Gamma}-\tilde{X}$; k_y along $\bar{\Gamma}-\bar{K}$ and k_z along $\tilde{\Gamma}-\tilde{Z}$, respectively, see Fig. 1d). The core level photoemission spectra (Fig. 1g) show sharp characteristic Sb_{4d}, K_{3p} and Hg_{5d} levels.

The electronic structures on the (001) surface

We first focus on the electronic structures on the (001) surface. From the 3D plot of the electronic structure (Fig. 2a) and stacked plot of the constant energy contours (CECs, Fig. 2b), one clearly see the electronic bands near $\bar{\Gamma}$ are hole-like. The six-fold rotational symmetry of the CECs further confirms the (001) surface cleavage. The diminished intensity on the Fermi surface (Fig. 2a-c) and the band dispersion measurements (Fig. 2f) confirmed that the Fermi-energy resides at the top of the valance band. In addition, both the CECs (Fig. 2c) and dispersions along high-symmetry direction $\bar{K}$-$\bar{\Gamma}$-$\bar{K}$ and $\bar{M}$-$\bar{\Gamma}$-$\bar{M}$ (see Fig. 2e(i)-(ii)) show excellent agreement with the *ab-initio* calculations (Fig. 2d and Fig. 2f(i)-(ii), respectively).

According to the band structure calculation[49], KHgSb is a fully gapped nonsymmorphic crystalline topological insulator with no surface states residing on the (001) surfaces. In order to prove this, we tuned the Fermi surface by introducing potassium atoms *in situ* onto the sample surface so that the absorbed potassium atoms on the surface would donate free electrons. After K-dosing, we could clearly observe the bottom of the conduction band and the top of the valence band simultaneously along both $\bar{K}$-$\bar{\Gamma}$-$\bar{K}$ and $\bar{M}$-$\bar{\Gamma}$-$\bar{M}$ directions (Fig. 2g(i)-(ii)). An indirect band gap of ~200 meV is observed with no signatures of in-gap surface states (Fig. 2h), agreeing with the calculations (Fig. 2e).

The electronic structures on the (010) surface

Next we demonstrate the detailed electronic structure on the (010) surface in Figure 3. Fig. 3a shows the stacking CECs. After inspecting CECs ranging from E_b=0~400meV, one could observe (see Fig. 3a,b) the quasi-one-dimensional Fermi surface disperses into two pieces when going to higher binding energies until new features with elliptical shape emerge at E_b~300 meV

(Fig. 3b(iv)). The broad agreements between the experiments (Fig. 3b) and *ab-initio* calculations (Fig. 3c) suggests the surface nature of the quasi-one-dimensional Fermi surface (Fig. 3b(i-iii)) and the bulk origin of the elliptical pockets (Fig. 3b(iv-v)), which can be confirmed by the photon energy dependent ARPES measurements (Fig. 3d, e).

In Fig. 3d, e, measurements along the $\tilde{X}$-$\tilde{\Gamma}$-$\tilde{X}$ direction (the CECs generated by this measurement in the k_x and k_y plane at E_b=0 and E_b=400meV) are plotted respectively. The quasi-one-dimensional states form straight lines dispersionless along the k_y direction (Fig. 3d), showing no photon energy dependence and thus proved their surface origin. On the other hand, at $E_b \sim 400$ meV where the quasi-one-dimensional CECs disappear, the bulk pockets emerge, showing strong k_y dispersion (Fig. 3e).

Finally, the electronic structures in Fig. 3a-e can be well explained by the surface and bulk band dispersions shown in Fig. 3f, g: while the surface state shows a sharp linear dispersion crossing the E_F (Fig. 3g, E_b=0 ~ 230meV, in the bulk gap), the bulk state (Fig. 3f, g, E_b>230meV) shows typical broad dispersion extending to high binding energy. Again, the position and shape of both surface and bulk states are in good agreement with our *ab-initio* calculations (see Fig. 3h for the bulk states calculation only and Fig. 3i for both the bulk and surface states; and more details can be found in supplementary information).

In summary, our measurement on the (010) cleaved surface of KHgSb has demonstrated the gapped bulk states with an in-gap surface state, in consistent with the *ab-initio* calculations that predict KHgSb as a nonsymmorphic topological crystalline insulator[49].

Resolving the delicate hourglass like surface fermion

In order to confirm that KHgSb is a glide reflection protected topological crystalline insulator, we now focus on the details of the dispersion of the quasi-one-dimensional surface state on the (010) surface.

As the glide reflection and time reversal symmetry guarantees the topological robust hourglass like surface fermion along the $\tilde{\Gamma}$-$\tilde{Z}$ direction[49] (Fig. 1b) and the surface quadruplets formed by time reversal conjugate partners disperse rapidly along the $\tilde{X}$-$\tilde{\Gamma}$-$\tilde{X}$ direction (and degenerate at $\tilde{\Gamma}$), the surface states form characteristic rhombohedral like dispersions close to the Fermi energy (see Fig. 1b for the illustration, focusing on features near Fermi level of the slice along $\tilde{X}$-$\tilde{\Gamma}$-$\tilde{X}$ direction). Between the two time reversal invariant momenta at $\tilde{\Gamma}$ and $\tilde{Z}$, the degeneracies are lifted and the glide reflection forces the switching of the two internal branches, forming hourglass like dispersion with the crossing point (the “leakage hole” of the

hourglass) pinned at certain momenta along $\tilde{\Gamma}$-$\tilde{Z}$ line in the reciprocal space. Further away from the crossing point, the two internal surface branches further separate, eventually forming a degeneracy point with their pseudo Kramers counterparts at $\tilde{Z}$, and showing a small gap between the upper and lower degenerate branches (Fig. 1b).

In the ARPES measurements of the electronic structures, we first investigate the evolution of surface states' dispersions parallel to the $\tilde{X}$-$\tilde{\Gamma}$-$\tilde{X}$ direction at different k_z values, which are shown in Fig. 4a(i-iv) (with their k_z positions marked on Fig. 4d, respectively). To better visualize the details of dispersions, the momentum 2nd derivative of the spectra intensity of dispersions are illustrated in Fig. 4b(i-iv) along with the schematics that show the surface state dispersion evolutions.

Comparing these surface dispersion (Fig. 4b) to the *ab initio* calculation results (Fig. 4c), we find they show nice agreement: Firstly, the most prominent feature in the no. 1 cut (k_z=0, at $\tilde{\Gamma}$) is the rhombohedral shaped dispersion near the Fermi energy formed by the surface states. As discussed above, this feature is generated by the quadruplets containing two separate pairs of conjugated surface state branches (highlighted by the red and blue guidelines; same below), each forming a Kramers degeneracy at $\tilde{\Gamma}$ (Fig.4a(i),b(i),c(i)). In the no. 2 cut (k_z=0.2 Å^{-1}, away from $\tilde{\Gamma}$), the surface states change dramatically and the degeneracy of the two Kramers degeneracies are lifted while the two internal branches still intersect with each other, forming a smaller rhombohedral feature (Fig.4a(ii),b(ii),c(ii)). The intersections of the two inner branches are removed as the slice goes further away from $\tilde{\Gamma}$ (no. 3 cut, k_z=0.4 Å^{-1}) and the two upper surface state branches and the bottom two surface state branches (pseudo Kramers doublets) gradually disperse together. Thus in no. 3 cut the rhombohedral feature disappears and a small gap appears between the pseudo Kramers doublets (Fig. 4a(iii),b(iii), c(iii)). Eventually, when the slice cuts across $\tilde{Z}$ (no. 4 cut, k_z=0.6 Å^{-1}), the small gap increases a little bit while the pseudo Kramers doublets become degenerate from a combined effect from both the time reversal symmetry and the glide reflection (Fig. 4a(iv), b(iv), c(iv)). Even though the predicted small gap between the pseudo Kramers doublets as well as its internal degeneracy is too small compared to the resolution of the ARPES measurements, the overall band dispersions and the evolution trend agree well with the calculation (Fig. 4c).

To reveal the hourglass like dispersion of the surface state quadruplets, we extract their dispersion along the $\tilde{Z}$-$\tilde{\Gamma}$-$\tilde{Z}$ direction in Fig. 4d. From the dispersion of the bulk valence band we could clearly identify the high symmetry points $\tilde{\Gamma}$ and $\tilde{Z}$. The dispersion of the weak surface state is tracked and highlighted by the red and blue curves (Fig. 4e). From the pattern

of the dispersion we could extract two (highly distorted) hourglass shapes from $\tilde{Z}$ to $\tilde{\Gamma}$ and $\tilde{\Gamma}$ to $\tilde{Z}$, which can evolved to a typical hourglass configuration (Fig. 4f) via continuous deformation (also see the movie clip in the supplementary information) and thus show their topological equivalence.

Conclusion

In summary, our ARPES measurements on KHgSb revealed its unique electronic structures on the (001) and (010) surfaces; and the agreements between experiments and the *ab-initio* calculations on both surfaces establish that KHgSb is the first nonsymmorphic crystalline symmetry protected topological insulator, hosting glide reflection protected topological hourglass fermion surface state on its side (010) surface. This discovery enriches the understanding of symmetry protected topological quantum states and will open the door in searching exotic topological quantum states and new fermions protected by other symmetries.

Acknowledgements:

This work is supported by grant from Chinese Academy of Science-Shanghai Science Research Center, Grant No: CAS-SSRC-YH-2015-01. Y.L.C. acknowledges the support from the Engineering and Physical Sciences Research Council Platform Grant (Grant No. EP/M020517/1) and Hefei Science Center Chinese Academy of Sciences (2015HSC-UE013). Z.K.L. acknowledges the support from the National Natural Science Foundation of China (11674229). J.J. acknowledges the support of the National Research Foundation, Korea, through the SRC Center for Topological Matter (No. 2011-0030787). C.C. acknowledges the support of the China Scholarship Council–University of Oxford Scholarship. H.F.Y. acknowledges financial support from the Bureau of Frontier Sciences and Education, Chinese Academy of Sciences. All authors contributed to the scientific planning and discussions. The authors declare no competing financial interests.

APPENDIX: MATERIALS AND METHODS

1. Sample synthesis:

K, Hg and Sb were weighed in the atomic ratio, 1:1:1 in an argon filled glove box. Sb pieces were powdered and mixed with K and Hg and transferred to a quartz crucible. The crucible was put inside a quartz tube which was then evacuated and sealed. The tube was kept in a muffle furnace at 370 ºC for 48 h. The temperature of the furnace was raised slowly (10 ºC/h) to avoid

sudden vaporization of K. The tube was broken inside the glove box and the content was powdered and transferred to an alumina crucible and sealed inside a tantalum tube. The tantalum tube was put in a quartz tube, evacuated and sealed. The content was heated to 900 °C for 10 h and cooled down to 475 °C with a rate of 3 °C/h. The temperature was kept constant at 475 °C for 175 h and then rapidly cooled to room temperature. Shiny crystals of KHgSb were obtained which were stored inside a glove box.

2. Angle-resolved photoemission spectroscopy:

Regular ARPES measurements were performed at the beamline I05 of the Diamond Light Source (DLS)，BL 10.0.1 of the Advanced Light Source, both equipped with Scienta R4000 analyzers and laser-ARPES system in the Institute of Physics, Chinese Academy of Sciences (IOP, CAS), with a Scienta DA30 analyzer. The measured sample temperature and pressure were 10 K (25K in IOP, CAS) and lower than 1.5×10^{-10} Torr, respectively. The angle resolution was 0.2° and the overall energy resolutions were better than 15 meV. The air sensitive KHgSb samples were first elaborately selected and prepared to realize two surfaces cleavage in a glove box with Ar filled and they were cleaved *in situ* along the (001) and the (010) surfaces accordingly.

3. *Ab-initio* calculations:

The density-functional theory (DFT) calculations were performed by using the code of Vienna ab-initio simulation package (VASP) with projector-augmented-wave (PAW) potential[54]. In order to get accurate band structures, we have used the modified Becke-Johnson exchange potential[55] for the exchange-correlation energy. For calculating the surface state, the tight binding Hamiltonian matrix was constructed by projecting the bulk Bloch wave functions to the maximally localized Wannier functions (MLWFs)[56]. The surface state was calculated in the half-infinite boundary condition by using the iterative Green's function method based on the tight model Hamiltonian[57].

References：

[1] M. Z. Hasan and C. L. Kane, Reviews of Modern Physics **82**, 3045 (2010).

[2] X.-L. Qi and S.-C. Zhang, Reviews of Modern Physics **83**, 1057 (2011).

[3] C. L. Kane and E. J. Mele, Phys Rev Lett **95**, 146802 (2005).

[4] B. A. Bernevig, T. L. Hughes, and S. C. Zhang, Science **314**, 1757 (2006).

[5] M. König, S. Wiedmann, C. Brüne, A. Roth, H. Buhmann, L. W. Molenkamp, X.-L. Qi, and S.-C. Zhang, Science **318**, 766 (2007).

[6] D. Hsieh, D. Qian, L. Wray, Y. Xia, Y. S. Hor, R. J. Cava, and M. Z. Hasan, Nature **452**, 970 (2008).

[7] H. Zhang, C.-X. Liu, X.-L. Qi, X. Dai, Z. Fang, and S.-C. Zhang, Nature Physics **5**, 438 (2009).

[8] Y. L. Chen *et al.*, Science **325**, 178 (2009).

[9] L. Fu, Phys Rev Lett **106**, 106802 (2011).

[10] T. H. Hsieh, H. Lin, J. Liu, W. Duan, A. Bansil, and L. Fu, Nat Commun **3**, 982 (2012).

[11] S. Y. Xu *et al.*, Nature Communications **3**, 1192 (2012).

[12] Y. Tanaka, Z. Ren, T. Sato, K. Nakayama, S. Souma, T. Takahashi, K. Segawa, and Y. Ando, Nature Physics **8**, 800 (2012).

[13] P. Dziawa *et al.*, Nat Mater **11**, 1023 (2012).

[14] Y. Tanaka, T. Sato, K. Nakayama, S. Souma, T. Takahashi, Z. Ren, M. Novak, K. Segawa, and Y. Ando, Physical Review B **87**, 155105 (2013).

[15] Z. Wang, Y. Sun, X.-Q. Chen, C. Franchini, G. Xu, H. Weng, X. Dai, and Z. Fang, Physical Review B **85**, 195320 (2012).

[16] Z. K. Liu *et al.*, Science **343**, 864 (2014).

[17] S. Y. Xu *et al.*, Science **347**, 294 (2015).

[18] A. J. Liang *et al.*, Chinese Phys B **25**, 077101 (2016).

[19] Z. Wang, H. Weng, Q. Wu, X. Dai, and Z. Fang, Physical Review B **88**, 125427 (2013).

[20] Z. K. Liu *et al.*, Nature Materials **13**, 677 (2014).

[21] M. Neupane *et al.*, Nat Commun **5**, 3786 (2014).

[22] S. Borisenko, Q. Gibson, D. Evtushinsky, V. Zabolotnyy, B. Buchner, and R. J. Cava, Phys Rev Lett **113**, 027603 (2014).

[23] H. Yi *et al.*, Sci Rep **4**, 6106 (2014).

[24] J. Liu and D. Vanderbilt, Physical Review B **90**, 155316 (2014).

[25] A. A. Burkov and L. Balents, Phys Rev Lett **107**, 127205 (2011).

[26] H. Weng, C. Fang, Z. Fang, B. A. Bernevig, and X. Dai, Physical Review X **5**, 011029 (2015).

[27] X. Wan, A. M. Turner, A. Vishwanath, and S. Y. Savrasov, Physical Review B **83**, 205101 (2011).

[28] D. Bulmash, C.-X. Liu, and X.-L. Qi, Physical Review B **89**, 081106 (2014).

[29] Z. K. Liu *et al.*, Nature Materials **15**, 27 (2016).

[30] B. Q. Lv *et al.*, Physical Review X **5**, 031013 (2015).

[31] S. Y. Xu *et al.*, Nature Physics **11**, 748 (2015).

[32] L. X. Yang *et al.*, Nature Physics **11**, 728 (2015).

[33] C. W. J. Beenakker, Annu. Rev. Condens. Matter Phys. **4**, 113 (2013).

[34] S. R. Elliott and M. Franz, Reviews of Modern Physics **87**, 137 (2015).

[35] R. Yu, W. Zhang, H. J. Zhang, S. C. Zhang, X. Dai, and Z. Fang, Science **329**, 61 (2010).

[36] C. Z. Chang *et al.*, Science **340**, 167 (2013).

[37] M. N. Ali *et al.*, Nature **514**, 205 (2014).

[38] F. F. Tafti, Q. D. Gibson, S. K. Kushwaha, N. Haldolaarachchige, and R. J. Cava, Nature Physics **12**, 272 (2016).

[39] L. K. Zeng *et al.*, Physical Review Letters **117**, 127204 (2016).

[40] J. He *et al.*, Phys Rev Lett **117**, 267201 (2016).

[41] J. Jiang *et al*., In preparation.

[42] S. A. Parameswaran, A. M. Turner, D. P. Arovas, and A. Vishwanath, Nature Physics **9**, 299 (2013).

[43] C.-X. Liu, R.-X. Zhang, and B. K. VanLeeuwen, Physical Review B **90**, 085304 (2014).

[44] K. Shiozaki and M. Sato, Physical Review B **90**, 165114 (2014).

[45] D. Varjas, F. de Juan, and Y.-M. Lu, Physical Review B **92**, 195116 (2015).

[46] C. Fang and L. Fu, Physical Review B **91**, 161105(R) (2015).

[47] K. Shiozaki, M. Sato, and K. Gomi, Physical Review B **91**, 155120 (2015).

[48] X.-Y. Dong and C.-X. Liu, Physical Review B **93**, 045429 (2016).

[49] Z. Wang, A. Alexandradinata, R. J. Cava, and B. A. Bernevig, Nature **532**, 189 (2016).

[50] A. Alexandradinata, Z. Wang, and B. A. Bernevig, Physical Review X **6**, 021008 (2016).

[51] J. Ma *et al.*, Science Advances **3**, e1602415 (2017).

[52] M. Ezawa, Physical Review B **94**, 155148 (2016).

[53] B. Yan, L. Muchler, and C. Felser, Phys Rev Lett **109**, 116406 (2012).

[54] G. Kresse and J. Furthmuller, Phys Rev B **54**, 11169 (1996).

[55] F. Tran and P. Blaha, Phys Rev Lett **102**, 226401 (2009).

[56] A. A. Mostofi, J. R. Yates, Y. S. Lee, I. Souza, D. Vanderbilt, and N. Marzari, Comput Phys Commun **178**, 685 (2008).

[57] M. P. L. Sancho, J. M. L. Sancho, and J. Rubio, Journal of Physics F: Metal Physics **14**, 1205 (1984).

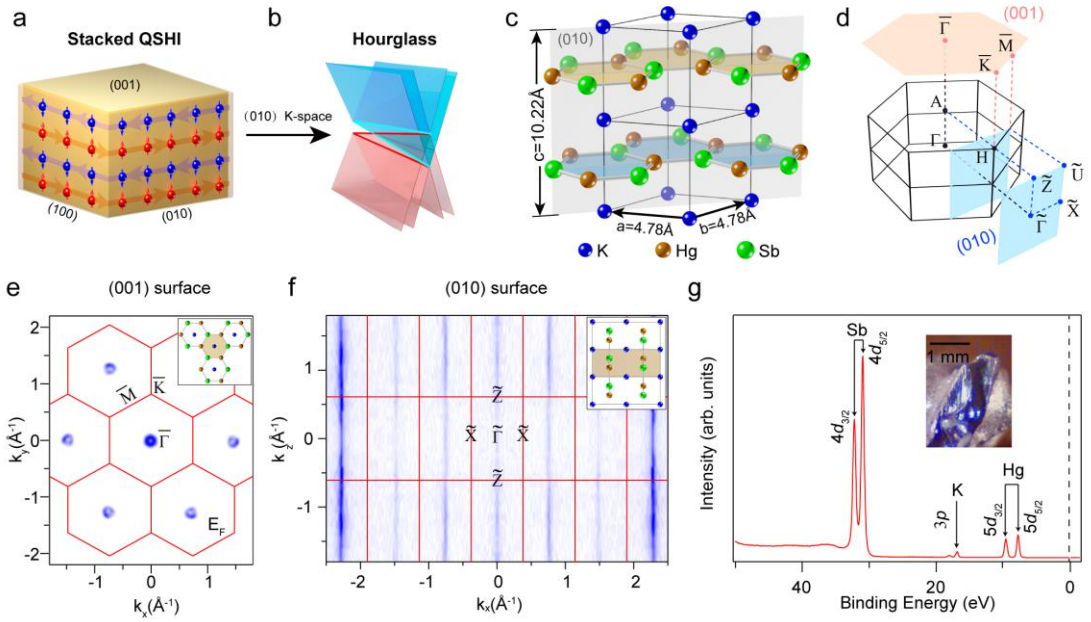

FIG. 1. (color online). **Novel surface modes and basic characteristics of KHgSb. a**, Schematic showing of the topological surface modes on the (100) and (010) surfaces of KHgSb. The four conducting branches of the surface mode on the (100) surface are almost dispersionless along c axis and paly as a 3D counterpart of the 2D quantum spin Hall insulator, whereas those on the (010) surface delicately disperse along c axis, giving rise to the hourglass like dispersion. **b**, A toy showing of the hourglass like dispersion on the (010) surface. **c**, Crystal structure of KHgSb. Two of the possible cleaved surfaces, e.g. (001) and (010) surfaces are highlighted with planes. A glide reflection exists on the (010) surface. **d**, Bulk and projected surface BZs of (001) and (010) surfaces. **e**, A large momentum scale of Fermi surface taken on the (001) surface. **f**, A broad Fermi surface from (010) surface. **g**, The integrated photoemission spectra from core levels of KHgSb with Sb $4d_{3/2}$ and $4d_{5/2}$, K $3p$, Hg $5d_{3/2}$ and $5d_{5/2}$ captured. Proper symmetrization is applied to the experimental data in order to have good comparison with calculation.

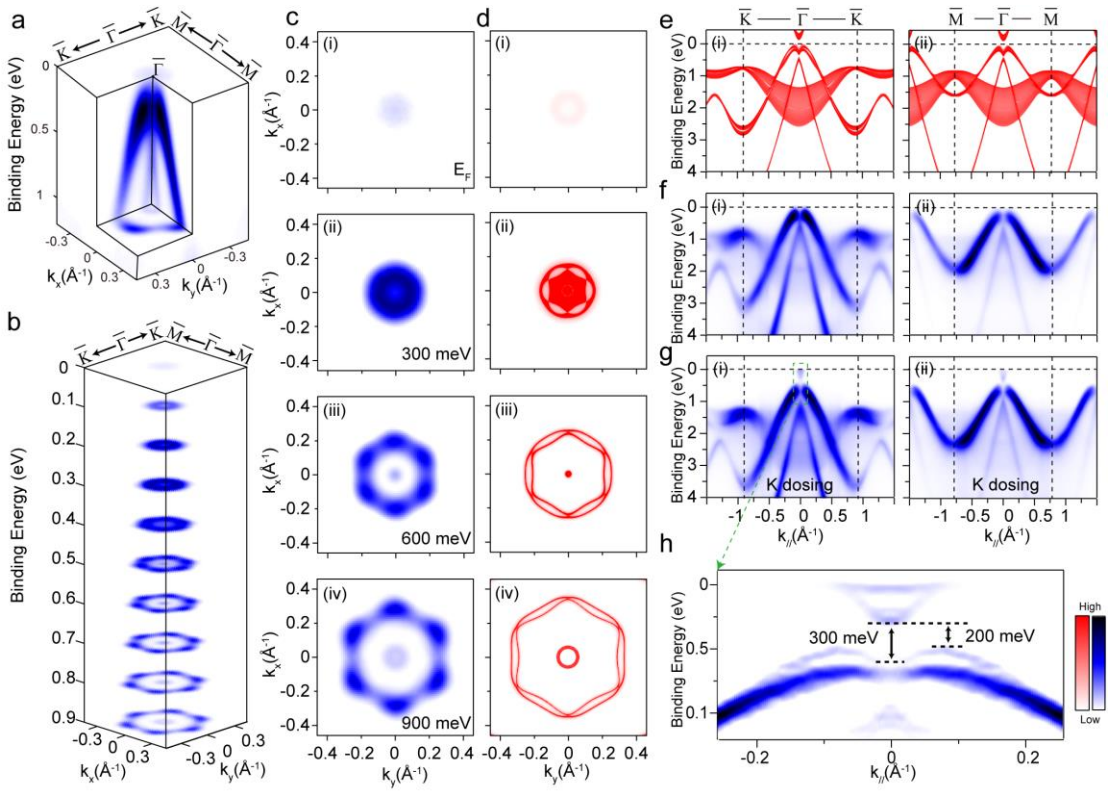

FIG. 2. (color online). **Basic electronic structures on the (001) surface of KHgSb. a**, A 3D illurstration of the in plane electronic stucture on the (001) surface of KHgSb. **b**， Dense CECs near Fermi energy. **c**, Selected CECs with binding energy E_b=0 meV (i), 300 meV (ii), 600 meV (iii) and 900 meV (iv) respectively. **d**, Calculated CECs in correspondence to those in **c**. **e**, Calculated band structures along two high symmetry directions $\bar{K}$-$\bar{\Gamma}$-$\bar{K}$ (i) and $\bar{M}$-$\bar{\Gamma}$-$\bar{M}$ (ii), respectively. The indirect band gap of the conduction and valence band is ~200 meV. **f**, Extracted band dispersions along both $\bar{K}$-$\bar{\Gamma}$-$\bar{K}$ (i) and $\bar{M}$-$\bar{\Gamma}$-$\bar{M}$ (ii) directions. **g**, The same band dispersions as those in **f** but with *in situ* potassium dosage to raise the Fermi energy. Full band gap is found without any signature of in-gap states in between the conduction and valence bands. **h**, The zoomed-in band dispersion in **g** (i). Second derivative method with respect to energy is employed. The experimental direct and indirect band gaps are noted. Proper symmetrization is applied to the experimental data in order to have good comparison with calculation.

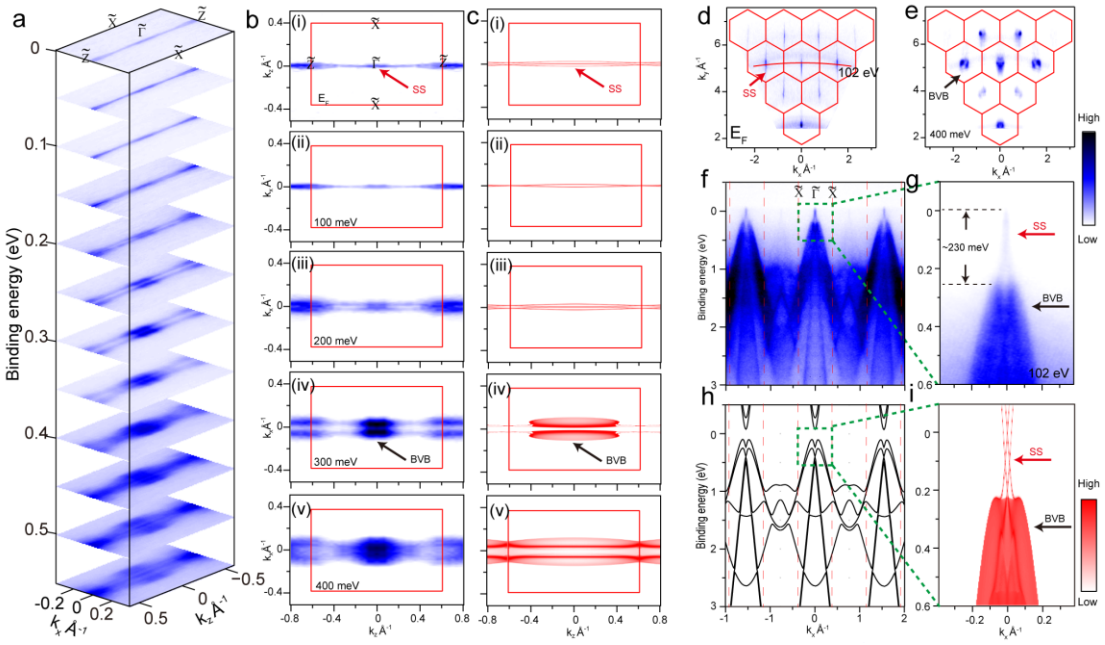

FIG. 3. (color online). **Basic electronic structures on the (010) surface of KHgSb. a**, A slice illustration of the CECs on the (010) surface of KHgSb. **b**, The selected CECs with binding energy E_b=0 meV (i), 100 meV (ii), 200 meV (iii), 300 meV (iv), 400 meV (v). **c**, The calculated CECs (i)-(v) with energies in accordance to those in **b**. The surface and the bulk parts of the contours are marked accordingly, BVB for bulk valence band and SS for surface state. **d**,**e**, A large momentum space scale of Fermi surface and CEC at a binding energy of 400 meV in k_x-k_y momentum space by collecting photon energy densely varied photoemission spectra along the $\tilde{X}$-$\tilde{\Gamma}$-$\tilde{X}$ direction. The one dimensional like dispersionless signatures in **d** indicate their surface nature and thus marked as surface states SS. The rounded hexagonal spots at each zone centers of the (001) surface BZs in **e** imply their photon energy variable sensitiveness and thus are bulk states from bulk valence band, marked as BVB. **f**, the extracted cuts along $\tilde{X}$-$\tilde{\Gamma}$-$\tilde{X}$ taken by linearly horizontaly polarized 120 eV photons with position denoted in **d**. **g**, The zoomed-in band dispersion in **f**. **h**, Calculated bulk bands along $\tilde{X}$-$\tilde{\Gamma}$-$\tilde{X}$ with $k_y = 0$. **i**, Calculated zoomed-in projected band dispersion along $\tilde{X}$-$\tilde{\Gamma}$-$\tilde{X}$.

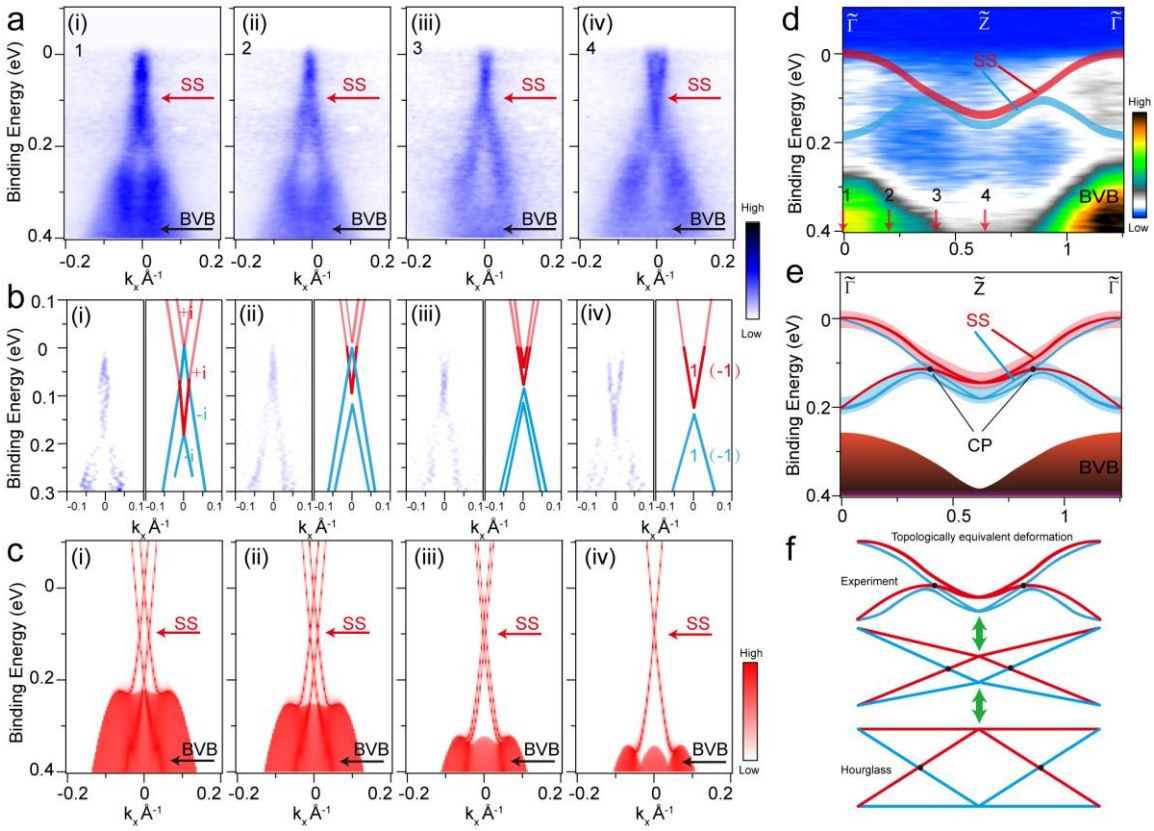

FIG. 4. (color online). **The resolution of the hourglass like surface fermion on the (010) surface of KHgSb. a**, The extracted band dispersions on the (010) surface which are parallel to the $\tilde{X}$-$\tilde{\Gamma}$-$\tilde{X}$ direction, covering half of the (010) surface BZ with $k_z \sim 0$ $Å^{-1}$(i), 0.2 $Å^{-1}$(ii), 0.4 $Å^{-1}$(iii), 0.6 $Å^{-1}$(iv), respectively. The exact position are noted in **d**. The surface state and the bulk valence bands are also indicated by SS and BVB. **b**, From (i)-(iv): each left panel is the MDC second derivative image in correspondence to that in **a**; each right panel schematically shows the evolution of the surface state, mimicing the behavior of each of the four surface state branches. The relatively light red lines indicates the bands which are not clearly observed. **c**, Calculated band dispersions with similar momentum positions of band dispersions in **a**. The surface state branches and the bulk states are also labelled as SS and BVB. **d**, The extracted band dispersion along the $\tilde{Z}$-$\tilde{\Gamma}$-$\tilde{Z}$ direction. The red and blue curves outline the trajectory of the surface state. **e**, A most possible configuration of the four surface state branches. The two internal branches interset each other and the total four surface state branches give rise to a pair of distorted hourglass fermions along the $\tilde{Z}$-$\tilde{\Gamma}$-$\tilde{Z}$ direction. **f**, The continuous deformation of

the distorted dispersion of hourglass fermions in **e** to eventually show their topologically equivalent to the well defined hourglass configurations.